Collective acoustic modes in various two-dimensional crystals by ultrafast acoustics: Theory and experiment

J.-F. Robillard, A. Devos,* I. Roch-Jeune, and P. A. Mante
Institut d'Électronique, de Microélectronique et de Nanotechnologie, Unité Mixte de Recherche CNRS 8520, Avenue Poincaré BP 69, F-59652 Villeneuve d'Ascq Cedex, France

(Received 6 June 2008; revised manuscript received 25 July 2008; published 15 August 2008)

We study the elastic properties of two-dimensional phononic crystals made of aluminum nanocube lattices. From the experimental point of view, collective modes resulting from the coupling between cubes inside the crystal are excited and time resolved using ultrafast acoustics. We derive a general theoretical model of the collective modes. From the analytical expression we discuss the influence of numerous crystal parameters on the detected frequencies. We then present experimental results on various samples which all exhibit an excellent agreement with the model. The theoretical description reveals that collective modes propagate along the sample surface. From that we propose to use such modes for measuring the in-plane elastic properties of thin films.

DOI: 10.1103/PhysRevB.78.064302 PACS number(s): 63.22.−m, 63.20.−e, 78.47.jc

I. INTRODUCTION

Picosecond ultrasonics (PU), also called ultrafast acoustics, is an optical method that enables the generation and detection of ultrasounds up to several hundred gigahertz far above conventional acoustic techniques.[1–3] This is possible thanks to the use of femtosecond laser pulses whose absorption in any opaque media thermally launches acoustic waves. The hypersound propagation modulates the optical reflectivity or transmittivity which is measured by a second delayed laser pulse. PU has been intensively used for probing elastic properties of thin films and multilayers down to a few nanometers.[4–8] From this point of view, femtosecond laser pulses in a pump-probe scheme achieve a sonar at the submicronic scale. Using the same setup, it is also possible to probe the elastic properties of nano-objects whose vibrations fall in a frequency range reachable by such an experiment. The detection of confined vibrational modes has been demonstrated on various systems such as colloids or quantum dots.[9–13]

All these studies did concern randomly disposed nano-objects with no mechanical coupling. Nanotechnology offers more and more opportunities to build artificial crystals whose unit cell is composed of one or more nano-object.[14–16] What about the elastic properties of such a crystal? This subject is a hot topic since it offers an unique way of designing the elasticity of a material by adjusting the individual properties of the dot and their arrangement within the crystal. From the theoretical point of view, the coupling between nano-objects leads to the formation of vibration bands of various nature. First the modes of the isolated object couple in "molecular" branches whose curvature is directly related to the coupling between dots. Second, low-frequency modes appear resulting from the displacement of one object with respect to others. Such modes are similar to acoustic phonons in an atomic crystal.

Until recently time-resolved studies performed on artificial crystals did not reveal collective modes but only individual vibrations.[15,16] Very recently we successfully applied ultrafast acoustics to probe both kinds of vibration on arrays of nanocubes made using *e*-beam lithography.[17] Aluminum nanocubes were mechanically coupled via an aluminum underlayer. We identified two distinct species of vibrations. The first modes are individual resonances of the cube; these are high-frequency oscillations which do not depend on the lattice parameter and whose period is linearly dependent on the cube width. This first result is similar to previous studies dedicated to colloïds or clusters. We also detected lower frequency oscillations which present different properties. The main point is the dependence of the period on both lattice parameter and cube width. We identified these oscillations as collective modes and proposed a simple elastic model for reproducing the experimental data. This report was a demonstration of the capability of picosecond ultrasonics for probing the elastic properties of such artificial crystals that are so-called phononic crystals. Several questions have been raised by this study in particular regarding the acoustical nature of the collective modes detected in these experiments. Here we focus on these collective modes for which we give a complete theoretical description. The generalized model predicts the detected frequencies for lattices whose symmetry, dot size, step, underlayer thickness, or composition can be modified. We then confront this model to experiments performed on numerous series of samples. An excellent agreement is found in any case. We learn more about the acoustical nature of these collective modes which are found to propagate along the surface in various directions. Finally we show how these modes could be used for measuring in-plane elastic properties of thin layers.

The paper is organized as follows: Section II gives details about the crystals' design and fabrication. We then describe the experimental setup and illustrate the experimental method on one sample series. In Sec. III we derive a theoretical model of the collective modes. From the analytical expression we discuss the influence of the different crystal parameters on the detected frequencies. Experimental results which exhibit an excellent agreement with the model are shown in Sec. VI. In Sec. V we discuss the possible interest of these modes for probing the in-plane elastic properties of thin films.

TABLE I. List of sample series. For each line a set of crystals with lattice parameters 400, 450, 500, 600, 700, 800, 1000, and 1200 nm are fabricated.

Sample series	Lattice type	Dot size d (nm)	Underlayer thickness h (nm)
A	square	200	100
B	hexagonal	200	100
C	square	100	100
D	square	200	20
E	square	200	400

II. EXPERIMENTAL DETAILS

A. Elaboration of the samples

The samples are built up on a Pyrex substrate. First an aluminum layer is deposited by *e*-beam metal evaporation. It is the underlayer on which cubes are deposited. Its thickness, designated as h in the following, is 20, 100, or 400 nm depending on the sample. The details concerning the samples used for this work are given in Table I. We use *e*-beam lithography to print the artificial crystals in a positive photoresist. Aluminum cubes are then built up by a second metal evaporation and a lift-off process. The high resolution of *e*-beam lithography (less than 10 nm) enables a precise control of the geometrical parameters and assures a low cube width dispersion. We designed square (series A and C–E) and hexagonal (series B) lattices of various cube widths (d). For a given cube width, underlayer thickness (h), and lattice symmetry, a set of crystals with various step sizes (a) is fabricated.

B. Experimental setup

The time-resolved experiments were conducted using a two-color pump and probe setup visible in Fig. 1. The laser source is a tunable Ti:sapphire oscillator which produces 120 fs optical pulses at a repetition rate of 76 MHz. The laser wavelength is tuned at 800 nm. The probe is focused into a β-baryum borate crystal for second-harmonic generation of a blue probe centered at 400 nm. This two-color scheme is needed since it was shown that the detection of the collective mode requires the probe wavelength to be less than the lattice constant of the crystals.[17] The time delay between pump and probe is controlled by a mirror associated to a 600 mm long translation stage which enables to scan up to 8 ns. To improve the signal detection the pump is chopped thanks to an acousto-optical modulator. This modulation is used for amplification of the probe signal in a lock-in scheme. The focal spot size of both pump and probe at the sample surface is about 50 μm so that excitation and detection concern a large collection of cubes.

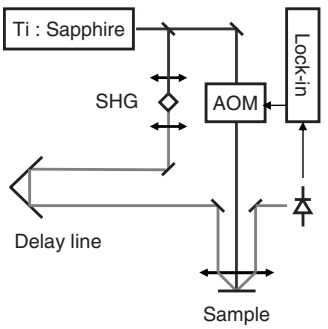

FIG. 1. Schematic diagram of the experimental setup. Second-harmonic generation (SHG) is used for producing a blue probe. Signal to noise ratio is improved by modulating the pump beam using an acousto-optic modulator (AOM) and a lock-in scheme.

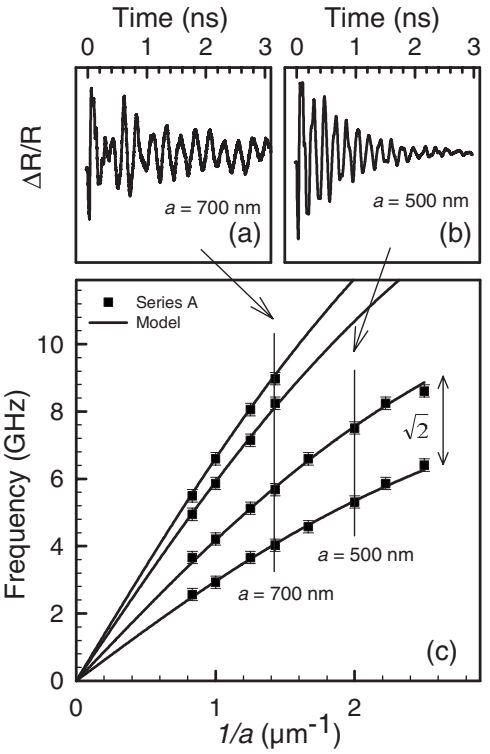

FIG. 2. Experimental method: for each lattice parameter a, we plot the measured frequencies as a function of $1/a$. The data obtained here on series A are then fitted using an analytical model described in the text.

C. Measurement and analysis of experimental data

Here we explain the analysis performed for each sample series. The energy of the pump beam is deposited at the sample surface due to the strong absorption of aluminum at 800 nm. The resulting heating of the aluminum surface creates a thermal stress. Because of the short laser-pulse duration acoustic displacements in the gigahertz range are impulsively excited in the structure.[2]

Any periodic displacement causes a modulation at the same frequency of the reflected probe beam intensity. The transient reflectivities of two samples from the series A with different lattice constants a are presented in Figs. 2(a) and 2(b). The signal includes several oscillating components. In the first 400 ps a weak oscillation whose period is 50 ps is visible. This component does not change with the lattice constant. It is related to the eigenmodes of the aluminum

cubes.[17] Let focus on the main signal visible on the nanosecond timescale. This oscillating signal includes several frequencies. It appears from the comparison of Figs. 2(a) and 2(b) that they strongly depend on the lattice step since the period of the signal for the $a=700$ nm sample is longer than for the $a=500$ nm sample. This paper is devoted to the analysis of these oscillations. In the following we will show that they originate from the propagation of a surfacelike mode. To investigate this mode the following method is used: For each sample type (lattice symmetry, cube width, underlayer thickness) we perform transient reflectivity measurements on the whole set of crystals with increasing lattice constant. The use of Fourier transform reveals up to four frequencies per crystal which are plotted as a function of the inverse of the lattice constant. This way we build the curves plotted in Fig. 2(c). The multiple frequencies detected order regularly as branches. The continuous lines are obtained from the model developed in Sec. III.

These plots have several relevant characteristics. First point, the upper branches of Fig. 2(c) can be deduced by scaling the lower one with remarkable factors $\sqrt{2}$,2 and $\sqrt{5}$. Second, each branch extends linearly to zero for lower and lower $1/a$ in a similar manner as an acoustic phonon branch. This is consistent with an acoustic origin of the oscillations. For experimental values of $1/a$ the curvature indicates the crucial role of the cube density per unit of surface. These characteristics are observed on each sample series described in Table I.

III. MODELING

Here we derive a theoretical description of the curves presented in Fig. 2 in the square lattice case. We then generalize it to any kind of two-dimensional crystal.

For doing that, we start from an usual dispersion relation for an acoustic mode written as

$$\omega(\vec{k}) = c(a) \,.\, \|\vec{k}\|, \tag{1}$$

where $\vec{k}$ is the wave vector and $c(a)$ the sound velocity of the mode. It is important to note that the collective nature of the mode appears in the dependence of the sound velocity on the lattice parameter. We first show that due to periodicity only a discrete set of wave vectors is permitted which explains that all the branches derive from the first one. Then we give an analytical expression for the sound velocity $c(a)$ as a function of a, d, and h which is valid for any crystal symmetry. Finally, we discuss the influence of each parameter on the frequencies.

A. Excitation of a discrete set of wave vectors

Due to the sample periodicity, the initial strain due to the pump light absorption has a similar periodic profile. Among all the normal modes of the structure the initial strain launched by the pump light will distribute on the subset of modes whose displacement comply with the sample periodicity. Let $\eta(\vec{r},t)$ be the strain field of one mode at position $\vec{r}$ and at time t. Then whatever the vector $\vec{A}$ of the direct lattice is, we can write

$$\eta(\vec{r}+\vec{A},t) = \eta(\vec{r},t). \tag{2}$$

Assuming $\eta(\vec{r},t)$ to be propagative parallel to the surface, we can write

$$\eta(\vec{r},t) = \eta_0 e^{i(\omega t - \vec{k}.\vec{r})}. \tag{3}$$

The respect of the condition (2) leads to $\vec{k}.\vec{A}=2n\pi$, where n is an integer. As a consequence for any crystal the only propagative modes excited are those whose wave vector $\vec{k}$ is a reciprocal-lattice vector.[18] In the case of a square lattice with a lattice constant equal to a, the permitted wave vectors $\vec{k}$ can be written as

$$\vec{k} = \frac{2\pi}{a}(i\vec{u}_x + j\vec{u}_y), \tag{4}$$

where i and j are integer numbers. The corresponding mode thus propagates in the (i,j) direction and its wave number $k_{i,j}$ is given by

$$k_{i,j} = \sqrt{i^2+j^2}\left(\frac{2\pi}{a}\right). \tag{5}$$

By reporting this in Eq. (1), we get for one crystal several frequencies between which we retrieve the observed remarkable factors between branches. The first four modes are those obtained with the directions (1,0), (1,1), (2,0), and (2,1). The ratios between the corresponding frequencies are 1, $\sqrt{2}$, 2, and $\sqrt{5}$ identical to those observed experimentally in Fig. 2(c). A first conclusion is thus that for any crystal, a same nondispersive acoustic wave is excited at several discrete wave vectors whose wave numbers vary (which leads to different frequencies) and which propagates along different crystal directions.

The discrete set of wave vectors is derived from the reciprocal lattice. For example in a hexagonal lattice the magnitude of the wave vectors $k_{i,j}$ are

$$k_{i,j} = \sqrt{i^2-ij+j^2}\left(\frac{2}{\sqrt{3}}\right)\left(\frac{2\pi}{a}\right). \tag{6}$$

In that case, the ratio between the two first branches is expected to be $\sqrt{3}$, given by the ratio between wave vectors in the (1,0) and (2,1) directions.

B. Velocity

Let us describe an analytical model in order to reproduce the velocity of the collective mode $[c(a)]$. Since the curvature is larger for high $1/a$ values, the velocity $c(a)$ decreases with the dot density at the sample surface. Here we show that such an effect can be explained by considering the mass loading of the cubes. Since all the branches are deduced from the first branch, we focus on the lower collective-mode frequency $(f_{1,0})$ and its dependence on the lattice constant a. We also assume that it is issued from a vibration of a unit cell described as a harmonic oscillator of stiffness K and mass M. The unit cell is composed of a cube and a square piece of the underlayer. We can write

$$f_{1,0} = \frac{1}{2\pi}\sqrt{\frac{K}{M}} = \frac{1}{2\pi}\sqrt{\frac{K}{\rho V}}, \tag{7}$$

where ρ is the mass density of aluminum and V the unit-cell volume. V can then be written as a function of a, d, and h the underlayer thickness. To go further, we first focus on the square lattice case

$$f_{1,0} = \frac{1}{2\pi}\sqrt{\frac{K}{\rho}}\frac{1}{\sqrt{ha^2 + d^3}}. \tag{8}$$

According to Eq. (1) the angular frequency of the lowest mode is

$$2\pi f_{1,0} = c(a)k_{1,0} = c(a)\frac{2\pi}{a}, \tag{9}$$

from which we can derive the formula of $c(a)$ valid for a square lattice

$$c(a) = \frac{1}{2\pi}\sqrt{\frac{K}{\rho}}\sqrt{\frac{a^2}{ha^2 + d^3}}. \tag{10}$$

We now examine the limit of infinitely spaced dots. In Fig. 2(c) we note a linear behavior of frequencies close to zero which defines a constant sound velocity for large a, designated by c_0 in the following. In other words

$$c_0 = \lim_{a\to\infty} c(a). \tag{11}$$

By introducing c_0 in Eq. (10), we get the sound velocity of the collective mode in the square lattice case

$$c(a) = c_0\sqrt{\frac{a^2}{a^2 + d^3/h}}. \tag{12}$$

c_0 here is the only adjustable parameter of the model.

This result can be generalized to any two-dimensional (2D) lattice. The general unit cell is defined by the vectors $\vec{a}_1$ and $\vec{a}_2$. The angle between vectors is designated by θ. It is straightforward to reproduce the previous calculation by modifying the expression used for the unit-cell volume V in Eq. (7). This leads to the generalized sound velocity

$$c(a) = c_0\sqrt{\frac{a^2}{a^2 + d^3/h\ \sin\ \theta}}. \tag{13}$$

In the particular case of a hexagonal lattice, $\sin\theta = \sqrt{3}/2$.

The model can also be extended to a sample in which cubes and underlayer are composed of two different materials. In that case we distinguish ρ_c and ρ_u the mass density of the cube and underlayer, respectively. The sound velocity can then be written as a function of $\epsilon = \rho_c/\rho_u$:

$$c(a) = c_0\sqrt{\frac{a^2}{a^2 + \epsilon d^3/h\ \sin\ \theta}}. \tag{14}$$

C. Discussion

The frequencies $f_{i,j}(a)$ are given by combining the discrete wave vectors and the sound velocity in Eq. (1)

$$f_{i,j}(a) = \frac{1}{2\pi}c_0\sqrt{\frac{a^2}{a^2 + \epsilon d^3/h\ \sin\ \theta}}k_{i,j}. \tag{15}$$

An important point is that there is only one fitting parameter for the whole set of branches. The continuous lines on Fig. 2(c) are obtained using a velocity $c_0 = 3.07 \pm 0.1$ nm ps^{-1}. The agreement between experiments performed on series A and model is excellent.

From this model we can now examine the influence of the lattice symmetry, the cube width, and the underlayer thickness on the lattice frequencies. The lattice symmetry plays a major role in the determination of the set of discrete wave vectors which itself determines the ratios between branches. For example, we expect a $\sqrt{2}$ factor between the first two branches in a square lattice and $\sqrt{3}$ factor for a hexagonal one.

Second from Eq. (14), we show that curvature is governed by the factor $\chi = \epsilon d^3/(h\ \sin\ \theta)$. Indeed, for large a values, $c(a)$ in Eq. (12) approaches c_0 since d^3/h being negligible compared to a^2. On the contrary, for small value of a, d^3/h is not negligible and the sound velocity decreases, which manifests itself as a curvature of the branches. Such an effect is expected in any phononic crystal in which a band structure appears due to the interferences between multiple reflections. The cube size d plays a major role on the branch curvature. The larger the cubes are, the more pronounced the curvature is expected. We also note that the thinner the underlayer is, the larger the curvature is. Furthermore, increasing the cube mass density produces similar effects. Each of these three influences can be understood by referring to the mass loading effect induced by the cubes. The curvature is governed by the impact of the cube mass on the unit-cell mass. The heavier the cube is, the more pronounced the curvature is.

The lattice symmetry should also affect the curvature of the branches. Indeed the curvature factor χ contains a $\sin\theta$ factor. This reveals that for two series whose cube width (d) and underlayer thickness (h) are identical, the $\sin\theta$ factor modifies the expression of $c(a)$. The smaller θ is, the more pronounced the curvature effect is.

IV. EXPERIMENTAL RESULTS

In this part we present the experimental results obtained on various series which let us test the model derived in Sec. III. Successively we compare the theoretical frequencies to measured results obtained on series in which the lattice symmetry, the cube width, or the underlayer thickness is modified.

A. Lattice symmetry

First we focus on the influence of lattice symmetry. In Fig. 3, we compare the two first branches measured on series A (square lattice) and series B (hexagonal lattice). The cube width and the underlayer thickness are identical in both series (Table I).

The lower branches of both sets are very close and well reproduced using the previous model with the same sound velocity $c_0 = 3.07 \pm 0.1$ nm ps^{-1}. This is in accordance with

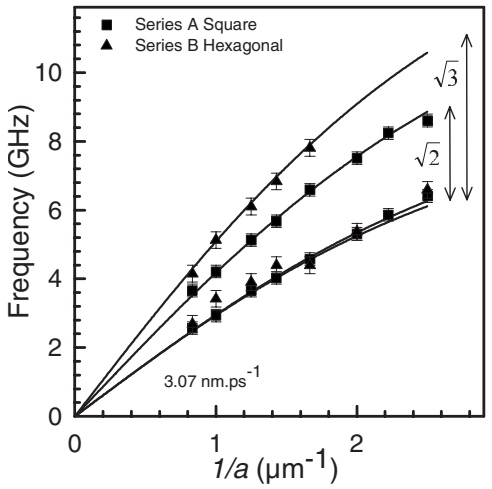

FIG. 3. Variation of the two lower frequencies with respect to the lattice parameter for hexagonal and square lattices.

the fact that for infinitely spaced cubes the surface has an intrinsic velocity which depends only on the substrate and underlayer system. In addition one should remark the minimal difference between modeling lines for hexagonal and square symmetries concerning the curvature which has been discussed in Sec. III C. Experimentally the effect of lattice symmetry on curvature is too small for being measurable. The most noticeable point is the difference in the factors needed for deducing the second from the first branch. The $\sqrt{2}$ factor needed in the square case is replaced by a $\sqrt{3}$ factor, as expected. This result confirms the role of the lattice symmetry in the selective excitation of a discrete vibration spectrum in the crystal.

B. Cube width

According to Eq. (12) for a given underlayer thickness, the cube width is expected to change the branch's curvature. To test this effect we used square lattices of 100 nm cubes (series D). Here again the same 100 nm aluminum underlayer is used. The lattice constants are similar to previous sets and only the cube width is changed. In Fig. 4(a) we compare the results measured on series D to those obtained on series A.

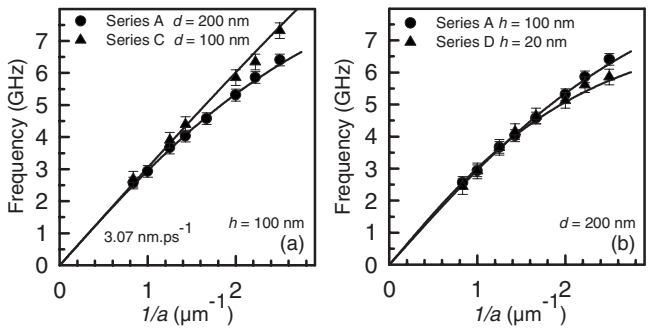

FIG. 4. (a) Variation of the lower surface mode frequency with respect to the lattice parameter for 100 and 200 nm cubes. (b) Variation of the lower surface mode frequency with respect to the lattice parameter for 20 and 100 nm thick underlayers.

For clearness, only the lower branch is plotted. While 200 nm cubes have a strong effect on the velocity $c(a)$ the 100 nm ones have a slight influence. The model accounts very well for this difference due to the cube width change. The initial velocity c_0 is still unchanged compared to previous results. These results confirm the role of the cubes as mass loading of the surface.

C. Underlayer thickness

Finally we explored the influence of the underlayer thickness. From the previous analysis the thickness is expected to act on the curvature. The consequence of the ratio between cube width and underlayer thickness is that a thinner layer gives a larger curvature. Three series of identical square lattices were built on different underlayers (series A, D, and E). The thicknesses are 20, 100, and 400 nm, respectively, while cube width is 200 nm. Only the results of series A and D are plotted on Fig. 4(b) for clarity. The harmonic-oscillator model is used to fit the data with a very good agreement. As predicted by the model, the thinner the underlayer is, the more pronounced the curvature is found.

V. DISCUSSION

The results presented in Sec. IV demonstrate that the theoretical description given in Sec. III is complete. For various lattice symmetry, cube width, or underlayer thickness the model reproduces the frequencies on the corresponding series from one fitting parameter c_0. Here we examine the meaning of the value extracted.

c_0 has been introduced as a limit value for the sound velocity of the collective mode in the extent of widely spaced cubes. While the perturbation of cubes gives a specific velocity to the surface mode the velocity, here c_0 does not depend on the cubes anymore. As propagation acts along the surface it can also be interpreted as the surface acoustic wave velocity in the underlayer/substrate stack. On series A–C we get $c_0=3.07\pm0.1$ nm ps^{-1} as expected since the underlayer and the substrate are identical for each series. On the contrary, the best fit of results obtained on series A, D, and E gives three different velocities c_0. It is thus found to be dependent on the thickness: the thinner the underlayer, the higher the velocity. These results are plotted in Fig. 5. It is important to note that this cannot be explained within the model. As shown below it gives additional information about the surface mode.

The velocity c_0 is in the same order of magnitude as the Rayleigh wave velocity of aluminum ($c_R=2.88$ nm ps^{-1}) and fused silica ($c_R=3.51$ nm ps^{-1}). It appears that for a thick aluminum underlayer, c_0 is close to the Rayleigh wave velocity of aluminum while for a thin layer the velocity increases and reaches the Rayleigh wave velocity of silica. This fact is natural since in these two limit cases the problem reduces to propagation at the surface of an isotropic half space.

To understand the evolution of c_0 as a function of h we performed finite element method (FEM) simulations.[19] By

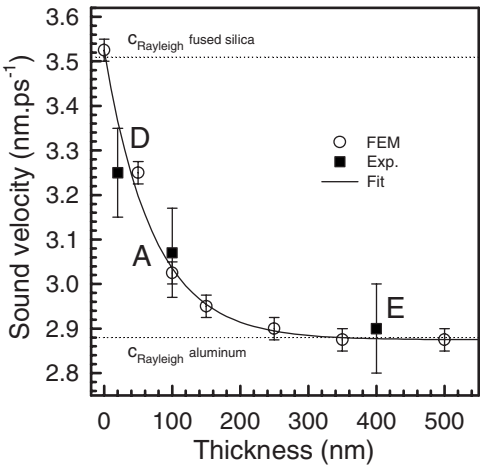

FIG. 5. Filled squares: Intrinsic velocity c_0 measured on samples series D, A, and E which only differ by the underlayer thickness (20, 100, and 400 nm respectively). Open circles: FEM simulation results of the surface wave velocity as a function of the underlayer thickness assuming a 200 nm acoustical wavelength. The continuous line is a rough extrapolation described in the text and given by Eq. (17).

means of a time domain algorithm an initial stress is propagated at the surface. The velocity is provided by the time of flight. The numerical results are plotted in Fig. 5. They fit very well an exponential decay from the Rayleigh wave velocity of silica to the one of aluminum.

Surface waves are damped in the direction normal to the surface over a distance of a few acoustical wavelengths. Thus whatever the precise displacement of the surface mode described here is, it is expected to extend over both aluminum layer and silica substrate. Indeed by the same mechanism as for wave vectors the acoustical wavelength is constrained to a discrete set whose higher is a. In our experiments the penetration depth of the surface mode is always in the same range as the layer thickness. Thus the intrinsic velocity c_0 is governed by the concerned proportion of layer and substrate.

Thanks to the small acoustic mismatch between aluminum and fused silica we can assume that the wave penetration depth δ is the same over both layer and substrate. Let us write the wave velocity as a mean between the Rayleigh wave velocity of the substrate and of the underlayer weighted by the thickness displaced

$$c_0(h) = \int_0^h c_R^U e^{-z/\delta} dz + \int_h^\infty c_R^S e^{-z/\delta} dz, \tag{16}$$

where c_R^U and c_R^S are the Rayleigh velocities of the underlayer and substrate, respectively. Finally, we get

$$c_0(h) = (c_R^S - c_R^U) e^{-h/\delta} + c_R^U. \tag{17}$$

This rough description shown in Fig. 5 as a continuous line agrees very well with both experimental and FEM results.

One can note that by measuring c_0 we reach the sound velocity of an acoustic wave which propagates in the plane of the underlayer/substrate stack. However, the previous analysis shows that it is possible to eliminate the influence of the underlayer. In Fig. 5 the extrapolation of the sound velocity in the limit $h \to 0$ gives the Rayleigh wave velocity of the silica substrate as expected. The same method could be applied to a thin layer deposited on a substrate. In that case, the sound velocity deduced from the limit $h \to 0$ would correspond to an in-plane property of the thin layer. That means that using such 2D lattices of nanocubes as a transducer, we can extract elastic properties of thin layers using a conventional ultrafast acoustic setup. It is particularly interesting since in ultrafast acoustics the geometry of the experience limits the exploration to longitudinal waves propagating perpendicularly to the layer. Due to that it is not possible to get all the elastic constants. What suggests the present study is that 2D lattices can be helpful for measuring in-plane properties on thin films. On isotropic materials by combining such a measurement to a conventional picosecond ultrasonic experiment we could access to all the elastic constants in submicronic layers. Furthermore, we have shown that various acoustic waves propagate along the surface in several directions. Experimentally these waves are clearly identified as successive branches. In the case of an anisotropic system, the sound velocity of these branches would differ. By measuring all the frequencies of the collective modes on such a sample, it should be possible to access to the different sound velocities.

VI. CONCLUSION

We have presented picosecond ultrasonic measurements performed on various 2D lattices of aluminum nanocubes. Collective acoustical modes issued from the mechanical coupling between dots are detected. We have derived an analytical model which fully reproduces the experimental data first in the square lattice case and then generalized to any 2D crystal. Numerous experimental data are fitted using only this model and one parameter which is the sound velocity of a surface acoustic wave of the underlayer/substrate stack. From the theoretical analysis, we show that several waves propagate along the sample surface in various directions defined by the reciprocal lattice. By studying the impact of nanocubes on sound velocity we thus get information about acoustic propagation in the underlayer. From that, we suggest that such lattices could be used for implementing an in-plane transducer needed in picosecond ultrasonics for reaching the complete set of elastic constants in thin layers using the conventional experimental setup.

*Arnaud.Devos@isen.fr

[1] C. Thomsen, J. Strait, Z. Vardeny, H. J. Maris, J. Tauc, and J. J. Hauser, Phys. Rev. Lett. **53**, 989 (1984).
[2] C. Thomsen, H. T. Grahn, H. J. Maris, and J. Tauc, Phys. Rev. B **34**, 4129 (1986).
[3] B. Perrin, C. Rossignol, B. Bonnello, and J.-C. Jeannet, Physica B (Amsterdam) **263**, 571 (1999).
[4] C. Rossignol, B. Perrin, S. Laborde, L. Vandenbulcke, M. I. D. Barros, and P. Djemia, J. Appl. Phys. **95**, 4157 (2004).
[5] H. Ogi, M. Fujii, N. Nakamura, T. Yasui, and M. Hirao, Phys. Rev. Lett. **98**, 195503 (2007).
[6] H. Ogi, M. Fujii, N. Nakamura, T. Shagawa, and M. Hirao, Appl. Phys. Lett. **90**, 191906 (2007).
[7] A. Devos, R. Cote, G. Caruyer, and A. Lefevre, Appl. Phys. Lett. **86**, 211903 (2005).
[8] O. B. Wright and T. Hyoguchi, Opt. Lett. **16**, 1529 (1991).
[9] T. D. Krauss and F. W. Wise, Phys. Rev. Lett. **79**, 5102 (1997).
[10] M. Nisoli, S. De Silvestri, A. Cavalleri, A. M. Malvezzi, A. Stella, G. Lanzani, P. Cheyssac, and R. Kofman, Phys. Rev. B **55**, R13424 (1997).
[11] A. V. Bragas, C. Aku-Leh, and R. Merlin, Phys. Rev. B **73**, 125305 (2006).
[12] A. V. Bragas, C. Aku-Leh, S. Costantino, A. Ingale, J. Zhao, and R. Merlin, Phys. Rev. B **69**, 205306 (2004).
[13] M. A. van Dijk, M. Lippitz, and M. Orrit, Phys. Rev. Lett. **95**, 267406 (2005).
[14] C. Kiely, J. Fink, M. Brust, D. Bethell, and D. Schiffrin, Nature (London) **396**, 444 (1998).
[15] G. A. Antonelli, H. J. Maris, S. G. Malhotra, and J. M. E. Harper, J. Appl. Phys. **91**, 3261 (2002).
[16] H.-N. Lin, H. J. Maris, L. B. Freund, K. Y. Lee, H. Luhn, and D. P. Kern, J. Appl. Phys. **73**, 37 (1993).
[17] J.-F. Robillard, A. Devos, and I. Roch-Jeune, Phys. Rev. B **76**, 092301 (2007).
[18] L. Brillouin, *Wave Propagation in Periodic Structures* (Dover, New York, 1953).
[19] ATILA Finite Element Code, Version 6.0.0, ISEN Lille, France.